

Thermal Stabilization of $Ce_xZr_{1-x}O_2$ Oxygen Storage Promoters by Addition of Al_2O_3 : Effect of Thermal Aging on Textural, Structural, and Morphological Properties

Roberta Di Monte,[†] Paolo Fornasiero,[‡] Stefano Desinan,[†] and Jan Kašpar^{*,†}

Dipartimento di Scienze Chimiche, Università di Trieste, Via L. Giorgieri 1, 34127 Trieste, Italy

José M. Gatica and José J. Calvino

Departamento de Ciencia de los Materiales e Ingeniería Metalúrgica y Química Inorgánica, Universidad de Cádiz, E-11510 Puerto Real (Cádiz), Spain

Emiliano Fonda

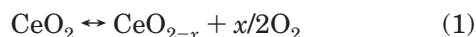
Synchrotron SOLEIL, L'Orme de Merisiers, Saint-Aubin, 91192 Gif-sur-Yvette Cedex, France

Received July 19, 2004

Thermal stability and dispersion of CeO_2 supported on Al_2O_3 is greatly improved by insertion of ZrO_2 into the CeO_2 lattice. It is shown that homogeneous nanosized $Ce_xZr_{1-x}O_2$ solid solutions can be prepared on the Al_2O_3 surface by using a citrate complexation synthesis method. Investigation of effects of $Ce_xZr_{1-x}O_2$ composition and loading of the $Ce_{0.2}Zr_{0.8}O_2$ phase on thermal stability and nanostructure of the prepared materials revealed that strong interactions between the supported phase and Al_2O_3 are induced by the high-temperature treatment. High contents of ZrO_2 , choice of the $Ce_xZr_{1-x}O_2$ precursors, and loading of the mixed oxide are critical factors leading to nanocomposite systems with high thermal and structural stability, consisting of particles of $Ce_{0.2}Zr_{0.8}O_2$ as small as 9–20 nm in close contact with a θ - Al_2O_3 matrix even after calcination at 1373 K. The enhanced stability of the present materials was confirmed also under hydrothermal conditions.

1. Introduction

As stringent quality standards for automotive emissions have been put in place by U.S. TIER 2 regulations,¹ the development of more efficient catalysts for abatement of exhaust emissions is essential. The so-called three-way catalyst (TWC), capable of converting, under proper stoichiometric air-to-fuel ratio (A/F), CO and hydrocarbons (HC) to CO_2/H_2O , and, simultaneously, reducing NO_x to N_2 , has been employed in automotive catalytic converters since 1980s.^{2,3} The fundamental working principles of the TWCs are the following: (1) use of Rh and Pt/Pd to promote, respectively, NO_x and CO/HC conversions; (2) addition of CeO_2 -based material to provide the so-called oxygen storage/release capacity (OSC), which is the ability of CeO_2 to maintain constant the oxygen partial pressure through the redox process



and (3) use of high-surface-area Al_2O_3 as support to achieve high dispersion of the noble metal. The so-called close coupled converter (CCC) is nowadays employed to improve efficiency (over 95–98% of pollutants conversion) of TWCs during cold start-up of the engine. This converter is mounted directly on the engine exhaust manifold, which exposes the catalyst to temperatures as high as 1373 K. Such high temperatures together with the required durability (over 120 000 miles) represent a strong challenge in the development of thermally stable catalytic materials. Sintering of the noble metal and deactivation of the OSC function due to CeO_2 particle growth have long been recognized as major TWC deactivation pathways.^{2,4} Ceria plays multiple roles in the TWCs,^{4,5} however, the OSC is certainly the most important one.⁶ Consistently, the efficiency of the TWCs is generally monitored by the on-board diagnostics (OBD) device, which employs a secondary oxygen sensor to detect deviations from the stoichiometric A/F, i.e., failure of the OSC component and hence of the TWC. At usual TWC working temperatures, reaction (1) is essentially related to the surface;⁷ even if formation

* To whom correspondence should be addressed. Fax: +39-040-5583903. E-mail: kaspar@units.it.

[†] Member of the European CONCORDE Coordination Action.

[‡] Also Center of Excellence for Nanostructured Materials of the University of Trieste.

(1) Bertelsen, B. I. *Platinum Met. Rev.* **2001**, *45*, 50.

(2) Taylor, K. C. Automobile catalytic converters. In *Catalysis: Science and Technology*; Anderson, J. R., Boudart, M., Eds.; Springer-Verlag: Berlin, 1984; vol. 5, pp 119–170.

(3) Taylor, K. C. *Catal. Rev. - Sci. Eng.* **1993**, *35*, 457.

(4) Kaspar, J.; Graziani, M.; Fornasiero, P. Ceria-Containing Three Way Catalysts. In *Handbook on the Physics and Chemistry of Rare Earths: The Role of Rare Earths in Catalysis*; Gschneidner, K. A., Jr., Eyring, L., Eds.; Elsevier Science B. V.: Amsterdam, 2000; Handbook on the Physics and Chemistry of Rare Earths, vol. 29, pp 159–267.

(5) Trovarelli, A. *Catal. Rev. - Sci. Eng.* **1996**, *38*, 439.

(6) Sohlberg, K.; Pantelides, S. T.; Pennycook, S. J. *J. Am. Chem. Soc.* **2001**, *123*, 6609.

of a CeO₂–ZrO₂ solid solution may enhance the mobility of the oxygen in the bulk, making more oxygen available.⁸ Thermal stabilization of highly dispersed nanosize particles of supported CeO₂ is therefore extremely important to achieve improved catalytic properties.⁹ Insertion of ZrO₂ into the CeO₂ lattice increases the thermal stability of CeO₂,¹⁰ however, due to the metastable nature of the CeO₂–ZrO₂ mixed oxides (CZMOs) of intermediate composition (CeO₂ content 20–80 mol %), the undesirable phase separation into CeO₂-rich and ZrO₂-rich phase occurs at high temperatures, as dictated by the CeO₂–ZrO₂ phase diagram.^{11,12}

Generally speaking, finely dispersed particles of CeO₂ can be obtained by calcination of Ce(NO₃)₃ impregnated on a support such as Al₂O₃, however, this creates an intimate contact between Al₂O₃ and the highly dispersed CeO₂ particles, facilitating the interaction between them. Upon aging, this easily leads to formation of CeAlO₃ that deactivates the OSC component.^{13,14} These previous observations and also patent claims (see for example U.S. patent 5,945,369, issued August 31, 1999) therefore clearly indicated the unsuitability of impregnation of CeO₂ on Al₂O₃ for production of effective OSC systems. Accordingly, it is usual practice to employ preformed CeO₂ or Ce_xZr_{1-x}O₂ particles to make TWCs. These particles are then suspended with Al₂O₃ and the other components, and finally wash-coated on the honeycomb. Recently, a number of papers addressed the issue of CeO₂–ZrO₂–Al₂O₃ materials with the aim of improving the thermal stability and redox properties of the CZMOs, however, complex and expensive synthesis strategies had to be employed to achieve materials with a reasonably good structural homogeneity of the CZMOs and thermal stability of the system;^{15–18} simple impregnation techniques easily lead in fact to CZMO phase segregated systems.¹⁹ A majority of these investigations addressed CeO₂-rich composition as the most interesting systems; in contrast, we have found that by doping CeO₂/Al₂O₃ systems with high contents of ZrO₂, the undesirable deactivation of CeO₂ can be minimized thereby leading to thermally stable OSC systems.²⁰

The present paper is a part of an extensive investigation aimed at developing novel thermally stable nanocomposite materials based on CeO₂–ZrO₂–Al₂O₃ systems, using different synthesis strategies. Here we investigate the synthesis conditions, and structural and morphological properties of nanocomposite Ce_xZr_{1-x}O₂/Al₂O₃ materials prepared by an incipient wetness deposition technique. A series of critical factors are disclosed that allow, using this simple and cost-effective methodology, effective stabilization of single-phase nanosized Ce_{0.2}Zr_{0.8}O₂ particles at the surface of Al₂O₃. Evidence for a mutual Ce_xZr_{1-x}O₂/Al₂O₃ thermal stabilization and interactions has, in fact, been observed.

Whereas the TWCs represent the major industrial application of these materials nowadays, CZMOs have also recently attracted wide interest in hydrocarbon reforming reactions, which is an important step of H₂ production from hydrocarbons, where thermal stability and controlled redox properties play a key role in enhancing the activity of the supported metals, adding further interest to these systems.^{21,22}

2. Experimental Section

Ce_xZr_{1-x}O₂ (YY wt %)/γ-Al₂O₃ (x = 1, 0.6, 0.2, 0) were prepared by using a modified citrate complexation method,²⁰ by impregnating to incipient wetness (i.w.) the resulting citrate-containing solution on γ-Al₂O₃ (BET surface area 186 m² g⁻¹, pore volume 1.03 mL g⁻¹). Hereafter the samples will be indicated as CZXX(YY)/Al₂O₃ where XX indicates the CeO₂ molar content relative to ZrO₂ (100, 60, 20, or 0 mol %) and YY indicates the amount (wt %) of CZMO relative to Al₂O₃. A typical preparation of the materials was carried out as follows. Ce(NO₃)₃·6H₂O (99.99%, Aldrich) was dissolved in water and mixed with a water solution of ZrO(NO₃)₂ (nominal content 20 wt % of ZrO₂, MEL Chemicals), then a water solution of citric acid (99.7%, Prolabo) was added. The ratio of metal cation to ligand was 1 to 2.1. The resulting solution was stirred at 340 K for 5 h, then at room temperature for 12 h, and finally concentrated to carry out an i.w. impregnation of the support. Some additional samples were also i.w. impregnated directly using the above Zr and Ce precursors. After impregnation, the material was dried at 393 K for 12 h, heated to 773 K at a heating rate of 3 K min⁻¹, and then calcined at this temperature for 5 h to obtain a white/pale yellow powder. Hereafter these samples are indicated as fresh ones. Catalysts were further aged by calcination in air at 973–1373 K for 5, 24, or 100 h. In selected experiments aging was performed under hydrothermal conditions (10% of H₂O) using a flow reactor in a flow of O₂ 5% in He (20 mL min⁻¹) that was passed through a water saturator before entering the catalyst bed (typically 0.8 g).

Powder XRD spectra were collected on a Siemens Kristalloflex Mod.F Instrument (Ni-filtered Cu Kα). The particle sizes are calculated with the Scherrer formula. Si (111) and (400) reflections were used as a measure of instrumental width in the range 20–35° and 60–70° (2θ). The first range was used to calculate the particle size of the CZMO and the latter was used for Al₂O₃. Alumina phase composition was evaluated by fitting the data using the Powder Cell software²³ using Al₂O₃ (and CZMO where appropriate) structural parameters taken from JPCDS file. The reliability of this procedure was also confirmed by a Rietveld fitting of the XRD patterns of the CZ20(13)/Al₂O₃ sample calcined at 1273 K. The RIETAN94

(7) El Fallah, J.; Boujana, S.; Dexpert, H.; Kiennemann, A.; Majerus, J.; Touret, O.; Villain, F.; Le Normand, F. *J. Phys. Chem.* **1994**, *98*, 5522.

(8) Fornasiero, P.; Di Monte, R.; Ranga Rao, G.; Kaspar, J.; Meriani, S.; Trovarelli, A.; Graziani, M. *J. Catal.* **1995**, *151*, 168.

(9) Zarur, A. J.; Ying, J. Y. *Nature* **2000**, *403*, 65.

(10) Cuif, J. P.; Blanchard, G.; Touret, O.; Seigneurin, A.; Marczy, M.; Quémeré, E. *Soc. Automot. Eng.* **1997**, 970463.

(11) Tani, E.; Yoshimura, M.; Somiya, S. *J. Am. Ceram. Soc.* **1983**, *66*, 506.

(12) Yashima, M.; Arashi, H.; Kakihana, M.; Yoshimura, M. *J. Am. Ceram. Soc.* **1994**, *77*, 1067.

(13) Shyu, J. Z.; Weber, W. H.; Gandhi, H. S. *J. Phys. Chem.* **1988**, *92*, 4964.

(14) Miki, T.; Ogawa, T.; Ueno, A.; Matsuura, S.; Sato, M. *Chem. Lett.* **1988**, 565.

(15) Fernandez-Garcia, M.; Martinez-Arias, A.; Hungria, A. B.; Iglesias-Juez, A.; Conesa, J. C.; Soria, J. *Phys. Chem. Chem. Phys.* **2002**, *4*, 2473.

(16) Fernandez-Garcia, M.; Martinez-Arias, A.; Iglesias-Juez, A.; Belver, C.; Hungria, A. B.; Conesa, J. C.; Soria, J. *J. Catal.* **2000**, *194*, 385.

(17) Masui, T.; Fujiwara, K.; Peng, Y.; Machida, K. I.; Adachi, G. Y. *Chem. Lett.* **1997**, 1285.

(18) Kozlov, A. I.; Kim, D. H.; Yezzerets, A.; Andersen, P.; Kung, H. H.; Kung, M. C. *J. Catal.* **2002**, *209*, 417.

(19) Yao, M. H.; Baird, R. J.; Kunz, F. W.; Hoost, T. E. *J. Catal.* **1997**, *166*, 67.

(20) Di Monte, R.; Fornasiero, P.; Kaspar, J.; Graziani, M.; Gatica, J. M.; Bernal, S.; Gomez Herrero, A. *Chem. Commun.* **2000**, 2167.

(21) Dong, W. S.; Jun, K. W.; Roh, H. S.; Liu, Z. W.; Park, S. E. *Catal. Lett.* **2002**, *78*, 215.

(22) Takeguchi, T.; Furukawa, S. N.; Inoue, M. *J. Catal.* **2001**, *202*, 14.

(23) Nolze, G.; Kraus, W. *Powder Diffr.* **1998**, *13*, 256.

program was used for the Rietveld analysis.²⁴

The high-resolution electron microscopy (HREM) data were obtained in a JEOL 2000EX instrument with 0.21 nm of structural resolution operating at 200 kV. For inspection in the microscope, the samples were deposited from a hexane suspension onto holey carbon coated Cu grids. The HREM images and electron diffraction patterns were digitized with a monochrome CCD camera, COHU-4910, and the digital analysis was conducted by means of the SEMPER 6+ software by Synoptics Ltd.²⁵ The digital diffraction patterns (DDP) correspond to the log-scaled power spectrum of the Fourier transform of the bi-dimensional intensity distribution in the digitized images.

XANES spectra at the L_{3} edge of Ce have been recorded in transmission mode at the D42 station of DCI storage ring (LURE, France). The monochromator used is a double crystal Si (311) with a 30% detuning. The ionization chambers were filled with air to reduce to a negligible extent the third harmonic contamination. The energy scale has been calibrated recording the K-edge of a metallic vanadium foil, and the calibration stability has been checked by recording the Cr edge during each scan by means of a photodiode after the second ionization chamber. The energy drift is less than 0.1 eV during the entire experiment. All samples were prepared for absorption by deposition of their finely ground powder on a Millipore membrane from a suspension in isopropyl alcohol and cyclohexane. The total absorption was limited to about 1 to limit the height of the Ce III white line. Scans have been performed with 0.25 eV steps in the XANES region (5700–5800 eV). XANES spectra have been first preedge corrected using the Victoreen equation. The spectra have been normalized using an edge jump estimated with the regression of a third-order polynomial above the edge and then the Lengeler–Eisenberger approximated energy dependence.

3. Results and Discussion

3.1. Choice of the $Ce_xZr_{1-x}O_2$ Precursors. With the aim of identifying the proper conditions for supporting the $Ce_xZr_{1-x}O_2$ phase onto Al_2O_3 , we have first performed the deposition of only ZrO_2 onto Al_2O_3 , using different ZrO_2 precursors. The advantage of using ZrO_2 instead of CZMO lies in the fact that the occurrence or absence of the t - ZrO_2 to m - ZrO_2 phase transformation upon calcination reveals the presence of intimate interactions between the ZrO_2 and Al_2O_3 phases. It must be recalled that a nanometric dimension of ZrO_2 plays a key role in the stabilization of the tetragonal phase, since the t - m phase transition is observed only above a critical particle dimension around 14 nm.²⁶ The most relevant results are summarized here for the citrate and nitrate ZrO_2 precursors.

Figure 1 reports the results of the textural characterization. Al_2O_3 features an isotherm of type II according to IUPAC definition,²⁷ with a hysteresis of type H3. The BHJ analysis of the desorption branch of the hysteresis reveals a broad pore distribution centered at 10–100 nm (Figure 1). The pore distribution is strongly modified after impregnation with zirconia precursors, and significant decrease of pore volume was observed.

(24) Izumi, F. Rietveld analysis programs RIETAN and PREMOS and special applications. In *The Rietveld Method*; Young, R. A., Ed.; Oxford University Press: Oxford, 1993; IUCr Monograph on Crystallography, pp 236–253.

(25) Bernal, S.; Botana, F. J.; Calvino, J. J.; Cifredo, G. A.; Perez-Omil, J. A. *Catal. Today* **1995**, *23*, 219.

(26) Baldinozzi, G.; Simeone, D.; Gosset, D.; Dutheil, M. *Phys. Rev. Lett.* **2003**, *90*, 216103/1.

(27) Sing, K. S. W.; Everett, D. H.; Haul, R. A. W.; Moscou, L.; Pierotti, R. A.; Rouquerol, J.; Siemianowska, T. *Pure Appl. Chem.* **1985**, *57*, 603.

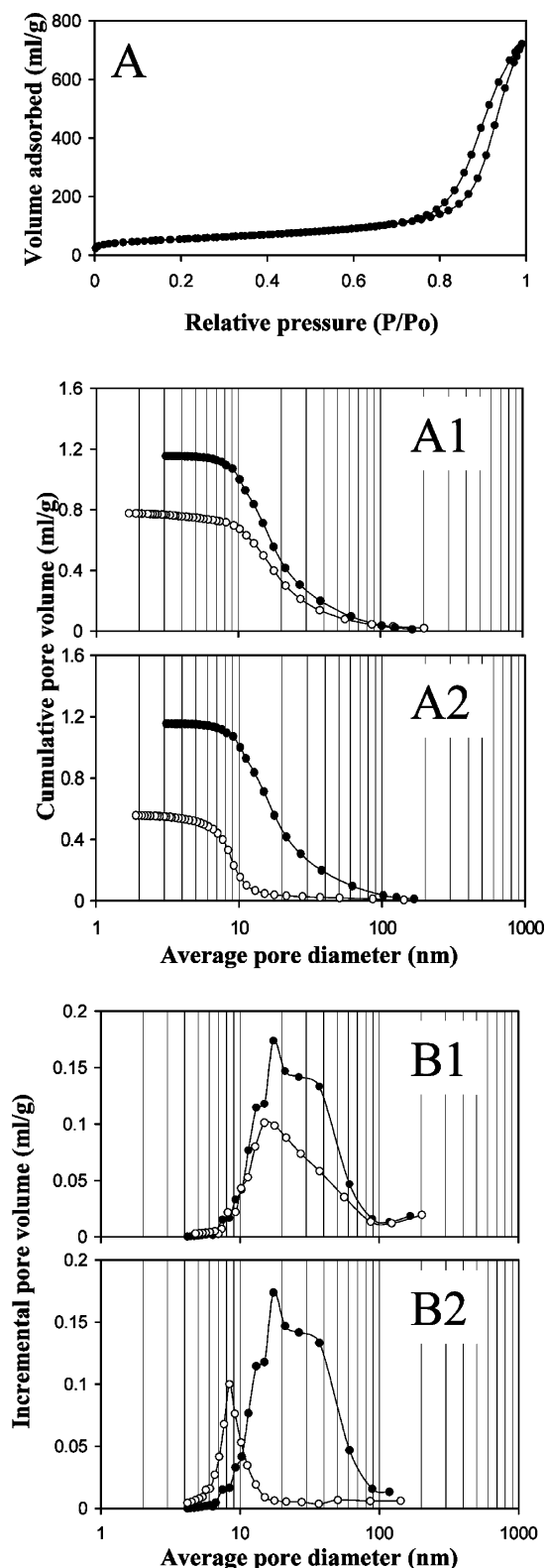


Figure 1. Effects of the impregnation procedure using i.w. technique with nitrate (1) or citrate (2) zirconia precursors on the textural properties of fresh ZrO_2/Al_2O_3 : (A) nitrogen adsorption–desorption isotherm at 77 K of Al_2O_3 ; (A1), (A2), effect of the impregnation on the cumulative pore volume; and (B1), (B2), effect of the impregnation on the pore distribution ((●) Al_2O_3 and (○) supported ZrO_2 (30 wt %)/ Al_2O_3).

The effects of deposition are quite remarkable when the citrate precursor is employed compared to nitrate; all the pores with a diameter higher than ca. 15 nm are totally annihilated, presumably due to their blocking

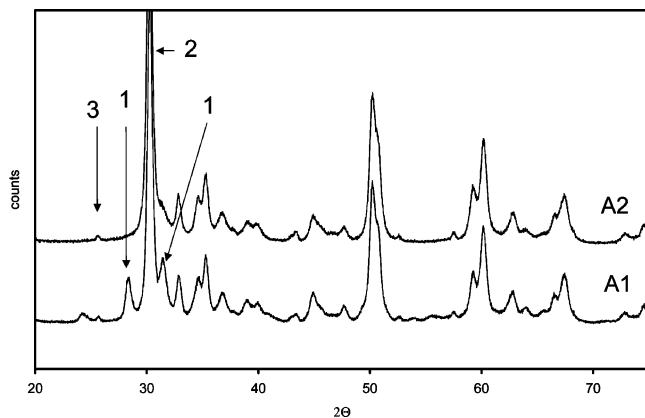


Figure 2. XRD patterns of $\text{ZrO}_2(30 \text{ wt } \%) / \text{Al}_2\text{O}_3$ samples after calcination for 5 h at 1373 K: (A1) nitrate precursors; (A2) citrate precursors. Peaks 1, 2, and 3 indicate characteristic reflections due to, respectively, $m\text{-ZrO}_2$, $t\text{-ZrO}_2$, and $\alpha\text{-Al}_2\text{O}_3$.

and/or partial filling with the supported phase. At the 30 wt % ZrO_2 loading a physical volume of 0.05 mL g^{-1} can be calculated for the ZrO_2 phase. The increase of the amount of pores centered at 8 nm suggests modification of the larger pores initially present in Al_2O_3 by the deposition process; attribution of such modification of pore distribution to the further calcination performed after the deposition is unlikely, since sintering would lead to an increase of pore diameters rather than a decrease. These effects should be related to the capability of citrate to strongly interact with the Al_2O_3 surface.²⁸

The importance of the synthesis methodology was confirmed when the samples were calcined at 1373 K for 5 h. XRD patterns of the two samples (Figure 2) revealed formation of a nanocomposite system with neatly segregated ZrO_2 and Al_2O_3 phases, and, most importantly, significant differences in the transformation of $t\text{-ZrO}_2$ into the monoclinic phase were observed (27 and 0% of $m\text{-ZrO}_2$ were detected using, respectively, nitrates and citrates as precursors). In comparison, unsupported ZrO_2 was completely transformed into $m\text{-ZrO}_2$ after such calcination treatment. It should be noticed that the inappropriateness of using nitrates as precursors was confirmed also by HREM investigation (data not shown) of a CZ20(13)/ Al_2O_3 sample, which featured after calcination at 1373 K larger particles than those achieved using the “citrate route” (10–30 nm vs 9–20 nm).

The overall data therefore clearly point out the importance of using a citrate precursor as an efficient route to induce a strong interaction between an Al_2O_3 and the ZrO_2 phase, favoring a nanometric dispersion of a $t\text{-ZrO}_2$ phase. On the basis of these results, citrate precursors have been employed in all the subsequent investigations.

3.2. Structural Transformation of the Al_2O_3 phase in CZXX(13)/ Al_2O_3 Samples. Effects of thermal aging on the structural and textural evolution of $\gamma\text{-Al}_2\text{O}_3$ and effects of impregnation of Al_2O_3 with ceria–zirconia at constant CZMO loading and different compositions were investigated by means of powder XRD and N_2 adsorption.

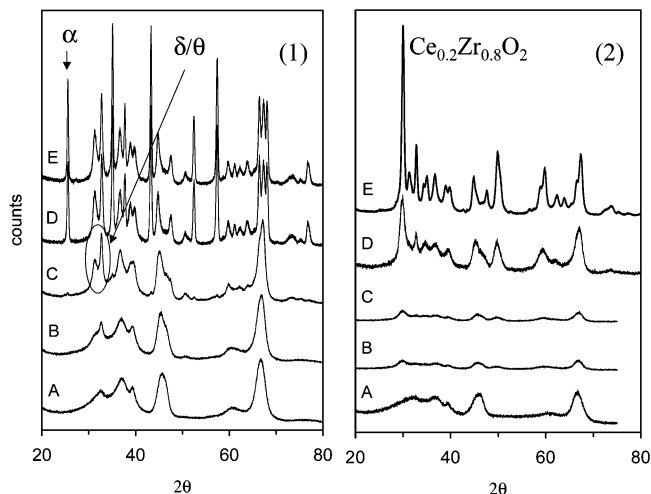
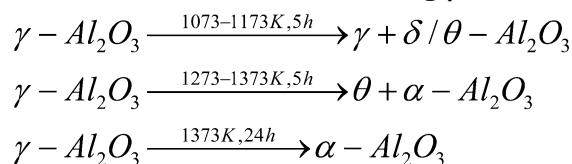


Figure 3. Effect of increasing calcination temperature on the XRD patterns of (1) Al_2O_3 and (2) $\text{Ce}_{0.2}\text{Zr}_{0.8}\text{O}_2(13 \text{ wt } \%) / \text{Al}_2\text{O}_3$. Calcination conditions: (A) 973 K, 5 h; (B) 1073 K, 5 h; (C) 1173 K, 5 h; (D) 1273 K, 5 h; (E) 1373 K, 5 h. Peaks characteristic of α - and $\delta/\theta\text{-Al}_2\text{O}_3$, and $\text{Ce}_{0.2}\text{Zr}_{0.8}\text{O}_2$ are indicated.

Scheme 1. Experimental Pattern for Thermal Transformation of the Starting $\gamma\text{-Al}_2\text{O}_3$



It is well-known that transition aluminas, such as $\gamma\text{-Al}_2\text{O}_3$, are metastable phases that upon increasing calcination temperature gradually transform into $\alpha\text{-Al}_2\text{O}_3$ ²⁹ with a great loss of specific surface area. Stabilization of the intermediate metastable phases depends on several factors, including textural properties, synthesis conditions, etc.,^{30,31} that may inhibit or slow the nucleation of $\alpha\text{-Al}_2\text{O}_3$. The transformation pattern with increasing the calcination temperature of the present $\gamma\text{-Al}_2\text{O}_3$ (sample B) was therefore considered first (Figure 3).

As observed from Figure 3 and summarized in Scheme 1, calcination progressively transforms $\gamma\text{-Al}_2\text{O}_3$ into δ (or θ) [Distinction of the δ and θ phases cannot not be performed from the XRD data by the above-quoted fitting procedure.] and finally to α phase, which start to be observed at 1073 and 1273 K, respectively. The latter is the only phase detected after 24 h at 1373 K. The addition of the CZMO phase to $\gamma\text{-Al}_2\text{O}_3$ confers an increased thermal stability to the transitional aluminas with respect to the CZMO-free support. Generally speaking, addition of either CeO_2 or ZrO_2 to Al_2O_3 can hinder thermal transformation of transitional aluminas to $\alpha\text{-Al}_2\text{O}_3$, but the true mechanism of this stabilization is not fully understood. Thin–monolayer dispersion of ZrO_2 was suggested to form over the $\delta\text{-Al}_2\text{O}_3$ that reconstructed to form bulk ZrO_2 only at very high

(29) Lippens, B. C.; Linsen, B. G.; de Boer, J. H. *J. Catal.* **1964**, *3*, 32.

(30) Pierre, A. C.; Elaloui, E.; Pajonk, G. M. *Langmuir* **1998**, *14*, 66.

(31) Tsukada, T.; Segawa, H.; Yasumori, A.; Okada, K. *J. Mater. Chem.* **1999**, *9*, 549.

(28) Hidber, P. C.; Graule, T. J.; Gauckler, L. J. *J. Am. Ceram. Soc.* **1996**, *79*, 1857.

Table 1. Textural and Structural Properties of $Ce_xZr_{1-x}O_2$ and $Ce_xZr_{1-x}O_2$ (13 wt %)/ Al_2O_3 Systems^a

sample	T_{cal}/K	time/h	BET surface area/ m^2g^{-1}	pore volume (mL/g)	particle size/nm (% phase)			
					Al_2O_3			CZMO
					γ	δ and θ	α	
Al_2O_3	973	5	186	1.084	4 (100)			
	1073	5	169	1.107	4 (55) 7 (45)			
	1173	5	122	0.877	4 (34) 12 (66)			
	1273	5	65	0.546	13 (76) 33 (24)			
		100	7	0.045	13 (19) 50 (81)			
	1373	5	58	0.478	14 (44) 38 (56)			
	24	12		>70 (100)				
CZ100/ Al_2O_3	773	5	180	0.920	4 (100)			
	973	5	168	0.918	7 (100) 6			
	1073	5	138	0.832	7 (53) 6 (47) 8			
	1173	5	113	0.765	8 (34) 9 (66) 11			
	1273	5	94	0.730	11 (100) 15			
	1273	100	36	0.275	14 (48) 63 (52) 31			
	1373	5	60	0.483	13 (92) 60 (8) 20			
	1373	24	32		14 (38) 52 (62) 28			
CZ60/ Al_2O_3	773	5	168	0.836	4 (100)			
	973	5	163	0.828	5 (100) 4			
	1073	5	159	0.900	5 (60) 9 (40) 6			
	1173	5	118	0.800	7 (28) 9 (72) 7			
	1273	5	76	0.541	8 (3) 10 (97) 12(90c)7(10t)			
	1273	100	38	0.287	14 (63) 24 (37) 16 (74c) 15 (26t)			
	1373	5	71	0.569	13 (100) 12(76c)13(24t)			
	1373	24	55		14 (93) 29 (7) 14(78c)12(22t)			
CZ20/ Al_2O_3	773	5	213	0.835	4 (100)			
	1073	5	146	0.846	5 (49) 4 (51) 5			
	1273	5	116	0.789	5 (15) 7 (85) 9			
	1373	5	68	0.586	13 (100) 11			
	1373	24	65	0.503	14 (98) 21 (2) 12			
CZ0/ Al_2O_3	773	5	225	0.820	4 (100)			
	1173	5			6 (52) 6 (48) 5			
	1273	5	116	0.733	6 (15) 7 (85) 10			
	1373	5	62	0.420	15 (97) 30 (3) 14			
	1373	24	48		12 (86) 33 (14) 15			
CZ20	773	5	24	0.028	6			
	1373	5	<5		35			
CZ60	773	5	44	0.037	5			
	1373	5	<5		20(85c)15(15t)			

^a c is a pseudo-cubic $Ce_xZr_{1-x}O_2$ phase and t is a tetragonal phase. All samples prepared by the citrate route.

temperatures, where appreciable migration of surface species can occur; this leads to loss of the interaction between the two phases with a concomitant formation of α - Al_2O_3 .³² The situation appears more complex for CeO_2 ; in fact some contradictory results have been found as far as textural and structural stabilization of Al_2O_3 by addition of CeO_2 are concerned.^{33–37} At low contents of the impregnated CeO_2 , a strong interaction between CeO_2 and Al_2O_3 occurs leading to significant formation of Ce^{3+} species that easily interact at high temperatures, particularly under reducing conditions, leading to formation of patches of $CeAlO_3$. This provides an effective way to prevent support sintering attributed to interfacial structural coherence of $CeAlO_3$ with alumina.^{38,39} Consistently, under oxidizing conditions the stabilizing

effect of CeO_2 is less effective, particularly at high loading.³⁷

Alumina phase compositions in CZXX(13)/ Al_2O_3 samples with different CZMO composition and calcined at increasing temperatures are reported in Table 1. The parallel decrease of the γ - Al_2O_3 content in the Al_2O_3 , CZ60(13)/ Al_2O_3 , and CZ100(13)/ Al_2O_3 with increasing calcination temperature clearly indicates that no appreciable interaction exists between this phase and the CeO_2 -rich mixed oxides. Some minor stabilization of γ - Al_2O_3 is observed for the CZ0(13)/ Al_2O_3 and CZ20(13)/ Al_2O_3 .

In contrast, an effective interaction between alumina and the supported CZMO phase is observed above ca. 1000 K, when δ/θ - Al_2O_3 are formed. It is worth noting that some α - Al_2O_3 is formed in the case of CZ100(13)/ Al_2O_3 at 1373 K, which is consistent with the high particle size of CeO_2 compared to the other CZMO compositions, leading to a minor interface area between the alumina and ceria phases.

(38) Humbert, S.; Colin, A.; Monceaux, L.; Oudet, F.; Courtine, P. Simultaneous Atmosphere and temperature cycling of three-way automotive exhaust catalysts. In *Catalysis and Automotive Pollution Control III*; Frennet, A., Bastin, J. M., Eds.; Elsevier: Amsterdam, 1995; Studies in Surface Science and Catalysis, vol. 96, pp 829–839.

(39) Oudet, F.; Bordes, E.; Courtine, P.; Maxant, G.; Lambert, C.; Guerlet, J. P. *Stud. Surf. Sci. Catal.* **1987**, *30*, 313.

(32) Horiuchi, T.; Teshima, Y.; Osaki, T.; Sugiyama, T.; Suzuki, K.; Mori, T. *Catal. Lett.* **1999**, *62*, 107.

(33) Ozawa, M.; Kimura, M. *J. Mater. Sci. Lett.* **1990**, *9*, 291.

(34) Morterra, C.; Magnacca, G.; Bolis, V.; Cerrato, G.; Barricco, M.; Giachello, A.; Fucale, M. Structural, morphological and surface chemical features of Al_2O_3 catalyst supports stabilized with CeO_2 . In *Catalysis and Automotive Pollution Control III*; Frennet, A., Bastin, J. M., Eds.; Elsevier: Amsterdam, 1995; Studies in Surface Science and Catalysis, vol. 96, pp 361–373.

(35) Haneda, M.; Mizushima, T.; Kakuta, N.; Ueno, A. *Bull. Chem. Soc. Jpn.* **1994**, *67*, 2617.

(36) Koryabkina, N. A.; Shkrabina, R. A.; Ushakov, V. A.; Moroz, E. M.; Lausberg, M. F.; Ismagilov, Z. R. *Kinet. Catal.* **1996**, *37*, 117.

(37) Piras, A.; Trovarelli, A.; Dolcetti, G. *Appl. Catal., B* **2000**, *28*, L77.

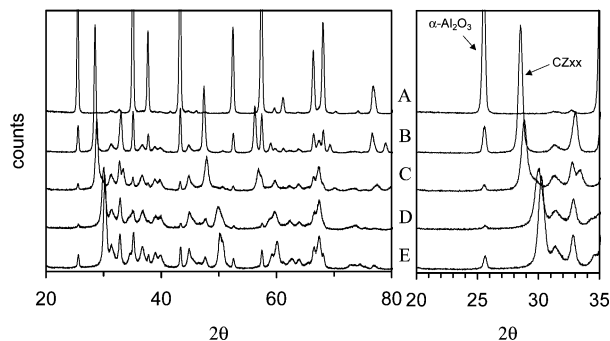


Figure 4. XRD patterns of $Ce_xZr_{1-x}O_2(13 \text{ wt } \%/Al_2O_3)$ after calcination at 1373 K for 24 h: (A) Al_2O_3 ; (B) $CeO_2(13 \text{ wt } \%/Al_2O_3)$; (C) $Ce_{0.6}Zr_{0.4}O_2(13 \text{ wt } \%/Al_2O_3)$; (D) $Ce_{0.2}Zr_{0.8}O_2(13 \text{ wt } \%/Al_2O_3)$; and (E) $ZrO_2(13 \text{ wt } \%/Al_2O_3)$.

As far as the textural properties are concerned, it is interesting to note that if the BET areas of the fresh CZXX(13)/ Al_2O_3 are normalized to 1 g of alumina, BET areas higher than that of the unloaded sample ($186 \text{ m}^2 \text{ g}^{-1}$) are estimated. Specifically, dividing the BET data in Table 1 by a 0.87 factor, the following values result: 207, 193, 245, $256 \text{ m}^2 \text{ g}_{Al_2O_3}^{-1}$. These larger numbers can be rationalized in the following way: by depositing CZMO particles a fraction of the initial alumina surface is covered, but also, at the same time, more surface is created by these surface-deposited particles. At equal loading, this process clearly depends on the composition of the CZMO.

To simulate the harsh conditions that can be met in a CCC, calcination was performed at 1373 K for 24 h. A neat effect of the composition of the CZMO phase on formation of $\alpha-Al_2O_3$ is observed (Figure 4). Pure Al_2O_3 is completely transformed to the α -phase, whereas the addition of CZXX decreases this conversion and stabilizes the alumina in the θ form, high ZrO₂ content is needed to prevent $\alpha-Al_2O_3$ formation. Assuming that the CZXX covers the Al_2O_3 surface as a film one layer thick,³² then a full monolayer coverage can be calculated as 36, 39, 43, and 44 wt % loading for respectively CZ100(13)/ Al_2O_3 , CZ60(13)/ Al_2O_3 , CZ20(13)/ Al_2O_3 , and CZ0(13)/ Al_2O_3 . The significant increase of $\alpha-Al_2O_3$ content with increasing the CeO_2 loading in the CZMO phase and the fact that the highest BET area ($66 \text{ m}^2 \text{ g}^{-1}$) was measured for the CZ20(13)/ Al_2O_3 suggest that the stabilization mechanism cannot be related to a pure physical blocking of the sintering mechanism due to a CZMO overlayer.

Finally, the value $66 \text{ m}^2 \text{ g}^{-1}$ measured after such severe calcination (1373 K, 24h) (Table 1) indicates that remarkably good thermal stability may be achieved by using this conceptually simple nanocomposite system.

3.3. Structural Transformation of the $Ce_xZr_{1-x}O_2$ phase in CZXX(13)/ Al_2O_3 Samples. Table 1 summarizes the structural data obtained for the different calcination temperatures. The metastable nature of the CZMOs favors phase segregation upon high temperature calcination, which makes detection of compositional inhomogeneities rather difficult. In fact, broad XRD patterns are typically observed on high-surface-area samples due to the small crystallite size. On the other hand, high-temperature calcination sharpens the XRD patterns due to sintering, but the presence of CeO_2 -rich and ZrO_2 -rich phases is often detected.⁴⁰ Observation

of a multiphase system can be attributed to either a phase segregation or presence of compositional inhomogeneities in the starting product. It is therefore difficult^{41,42} to assess the appropriateness of a synthesis methodology to produce a solid solution. However, a careful comparison of XRD patterns of differently synthesized $Ce_{0.5}Zr_{0.5}O_2$ mixed oxides allowed a criterion for detection of compositional homogeneity to be derived: no phase segregation was in fact observed after calcination of $Ce_{0.5}Zr_{0.5}O_2$ for 5 h at 1273 K, provided that appropriate synthesis methodology was employed.^{42,43} This criterion is therefore applied in the present work.

About 10% of a ZrO₂-rich impurity was detected in the CZ60(13)/ Al_2O_3 after calcination at 1273 K for 5 h, which is attributed to the presence of a compositional inhomogeneity in the fresh sample. A single-phase product was observed for the CZ20 phase in CZ20(13)/ Al_2O_3 . This is in agreement with previous observation that compositional inhomogeneity is favored at intermediate compositions.¹⁹ Equal degree of phase segregation is detected in the CZ60(13)/ Al_2O_3 after calcination at 1273 K for 100 h and in that observed after calcination at 1373 K for 5 h, indicating that the interaction generated in the present samples may slow the phase segregation (kinetic effect) without, however, affecting the thermodynamics of the process.

When the calcination temperature was increased to 1373 K, phase segregation in the CZ60(13)/ Al_2O_3 promptly occurred, indicating the unsuitability of such a CeO_2 -rich composition for high-temperature applications. Very importantly, no appreciable phase segregation was detected in CZ20(13)/ Al_2O_3 under such conditions, even for very long calcination times (100 h). The interaction with Al_2O_3 of the supported CZ20 mixed oxide strongly depressed its sintering, as indicated by the comparison with the average particle size detected in the unsupported $Ce_{0.2}Zr_{0.8}O_2$ (Table 1).

Some evidence has been reported by Mamontov et al. that the presence of heterogeneity at a nanophase level in CZMOs may lead to efficient OSC systems;^{41,44} in contrast, researchers from Toyota⁴⁵ have shown that increasing the homogeneity and ordering of the solid solution strongly enhances the OSC property. Consistently, the OSC values measured under similar experimental conditions (isothermal reduction with H_2) are respectively $750 \mu\text{mol } O_2/\text{g}_{CZMO}$ for an ordered and homogeneous $Ce_{0.5}Zr_{0.5}O_2$ ⁴⁵ and $470 \mu\text{mol } O_2/\text{g}_{CZMO}$ for the best nanophase-domain type of $Ce_{0.5}Zr_{0.5}O_2$ material.⁴¹ Whereas detection of the presence of nanodomains by conventional techniques may be difficult,⁴¹ it must be underlined that the presence of compositional nanosized inhomogeneities favors accelerated phase segregation for calcination at and above 1000 °C, allowing an easy detection by conventional XRD tech-

(40) Hori, C. E.; Permana, H.; Ng, K. Y. S.; Brenner, A.; More, K.; Rahmoeller, K. M.; Belton, D. N. *Appl. Catal., B* **1998**, *16*, 105.

(41) Mamontov, E.; Brezny, R.; Koranne, M.; Egami, T. *J. Phys. Chem. B* **2003**, *107*, 13007.

(42) Kaspar, J.; Fornasiero, P. *J. Solid State Chem.* **2003**, *171*, 19.

(43) Kaspar, J.; Fornasiero, P.; Balducci, G.; Di Monte, R.; Hickey, N.; Sergio, V. *Inorg. Chim. Acta* **2003**, *349*, 217.

(44) Dmowski, W.; Louca, D.; Egami, T.; Brezny, R. *Ceram. Trans.* **1997**, *73*, 119.

(45) Nagai, Y.; Yamamoto, T.; Tanaka, T.; Yoshida, S.; Nonaka, T.; Okamoto, T.; Suda, A.; Sugiura, M. *Catal. Today* **2002**, *74*, 225.

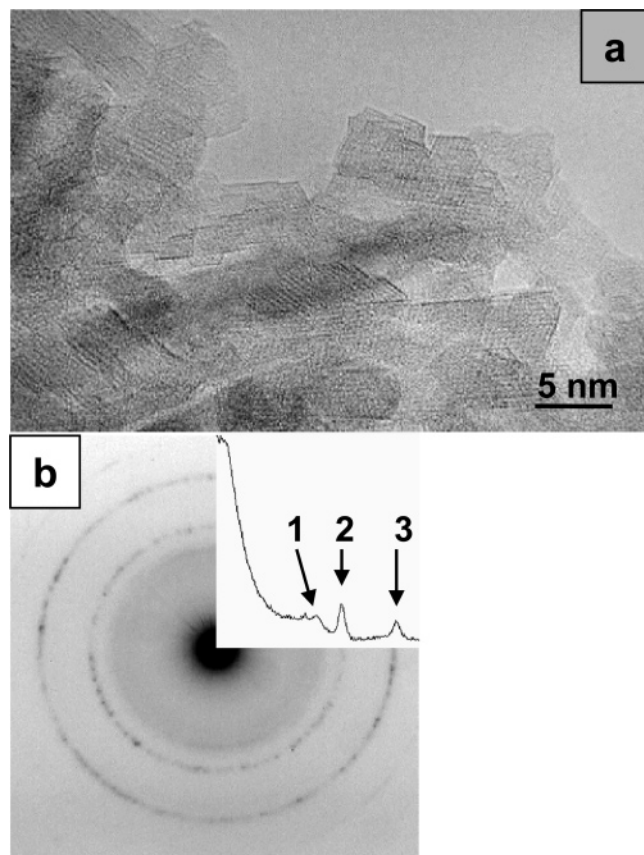


Figure 5. Representative HREM image (a) and electron diffraction pattern (b) of fresh $Ce_{0.2}Zr_{0.8}O_2$ (22 wt %)/ Al_2O_3 . The reflections observed in the intensity profile included in (b) can be indexed as (110)_{tetragonal} $Ce_{0.2}Zr_{0.8}O_2$ (1), (400)_{cubic} γ - Al_2O_3 (2), and (440)_{cubic} γ - Al_2O_3 (3).

nique.^{42,46} Importantly, the CeO_2 -rich component (about 80 mol %), which is formed by the phase segregation, is a sinterable material compared to other CZMO compositions;⁴⁷ this leads to a strong decline of dynamic-OSC.²⁰ This property, which is measured under cycling feedstream compositions (typically alternating pulses of CO and O_2), is closely related to the TWC application and is linked to the extent of surface area of the OSC material and therefore to its sinterability.^{40,48} This highlights the favorable properties of the present CZ20-(13)/ Al_2O_3 material.

3.4. HREM Analysis. Fresh and calcined samples were investigated by means of HREM and some representative results are shown in this section. This technique offers the possibility of obtaining fine structural details of the nanosized particles when dispersed onto supports as the materials are imaged at an atomic scale.⁴⁹

Figure 5 shows a HREM image representative of fresh samples. The presence of conglomerates of nanometer-

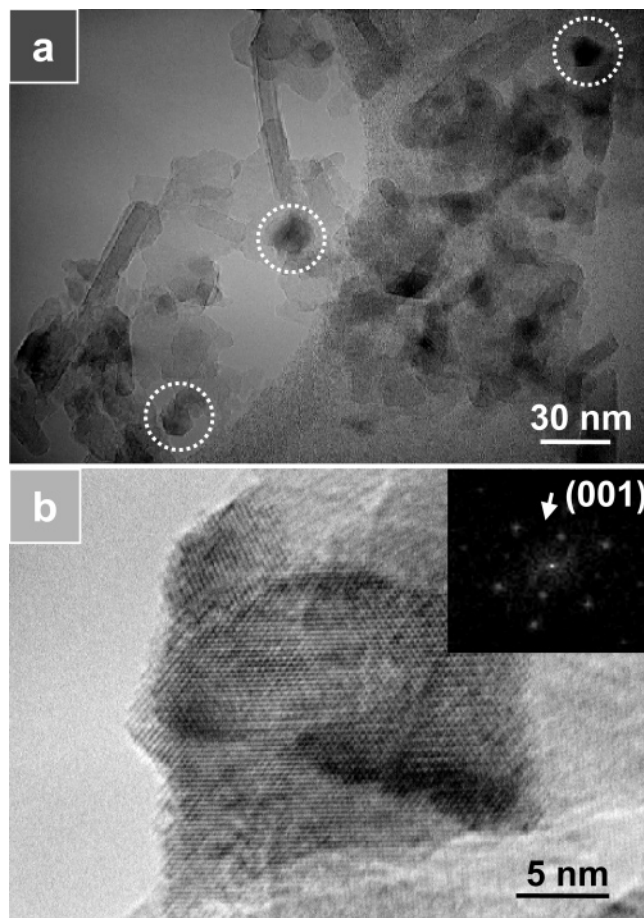


Figure 6. Representative HREM images of the $Ce_{0.2}Zr_{0.8}O_2$ - (13 wt %)/ Al_2O_3 sample calcined at 1373 K for 5 h. Some of the detected $Ce_{0.2}Zr_{0.8}O_2$ particles are indicated by a circle in (a). The digital diffraction pattern of these particles, like that included in figure (b), allows their unequivocal identification as $Ce_{0.2}Zr_{0.8}O_2$ tetragonal phase (see text for details).

sized alumina crystallites, like the one observed in this figure, is the most remarkable feature. Whereas single CZMO crystallites could not be detected, evidence for the presence of a CZMO phase has been obtained from electron diffraction patterns recorded on extended regions, tens of nm^2 in size. This is illustrated in Figure 5b, which shows that selected area electron diffraction patterns of fresh samples with CZMO contents up to 22 wt % feature several intense rings that can be assigned to γ - Al_2O_3 , as well as a more diffuse ring of reflections which can be assigned to CZMO crystallites with tetragonal structure. Both these electron diffraction results and lack of detection of distinct CZMO crystals in the HREM images suggest a high dispersion of the CZMO phase in the fresh samples.

The effect of the aging treatment at 1373 K has been investigated in detail on the CZ20(13)/ Al_2O_3 sample. According to low-magnification TEM images, like those presented in Figure 6a, after this treatment the CZMO phase is present in the form of nanometer-sized particles in close contact with the alumina support. The identification of the chemical nature of these particles was achieved by means of digital analysis of the HREM data. Digital diffraction patterns (DDPs) were obtained, by applying Fourier transform to the digitized images, on which a precise measurement of distances and angles between planes in the particles could be performed. The

(46) Kaspar, J.; Fornasiero, P. Structural properties and thermal stability of ceria-zirconia and related materials. In *Catalysis by Ceria and Related Materials*; Trovarelli, A., Ed.; Imperial College Press: London, 2002; Catalytic Science Series, vol. 2, pp 217–241.

(47) Janvier, C.; Pijolat, M.; Valdivieso, F.; Soustelle, M.; Zing, C. *J. Eur. Ceram. Soc.* **2001**, *18*, 1331.

(48) Boaro, M.; de Leitenburg, C.; Dolcetti, G.; Trovarelli, A. *J. Catal.* **2000**, *193*, 338.

(49) Bernal, S.; Baker, R. T.; Burrows, A.; Calvino, J. J.; Kiely, C. J.; Lopez-Cartes, C.; Perez-Omil, J. A.; Rodriguez-Izquierdo, J. M. *Surf. Interface Anal.* **2000**, *29*, 411.

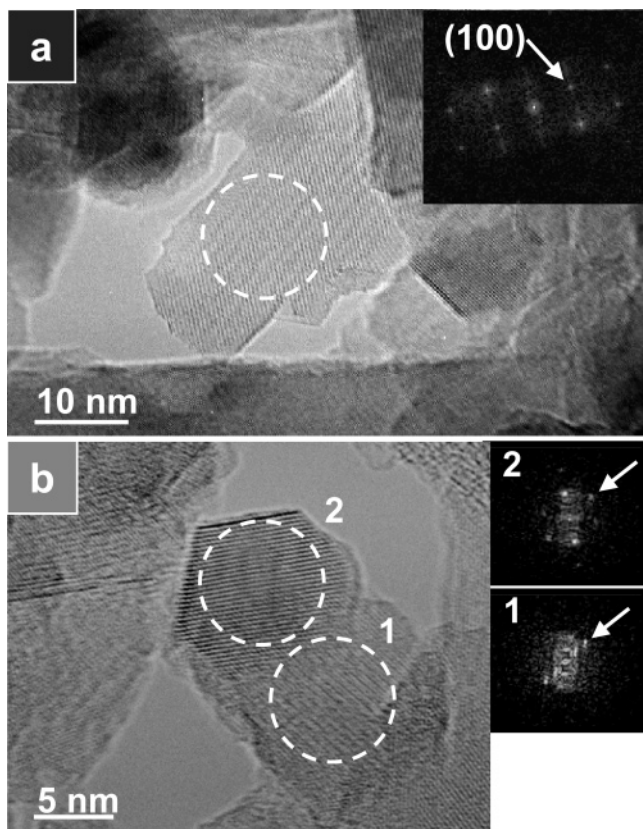


Figure 7. HREM study of $\text{Ce}_{0.2}\text{Zr}_{0.8}\text{O}_2(13 \text{ wt } \%) / \text{Al}_2\text{O}_3$ calcined at 1373 K for 5 h. (a) HREM image showing a crystallite of $\theta\text{-Al}_2\text{O}_3$ (encircled) as confirmed by means of DDP (in the inset) in which (100) planes with 0.55 nm spacing can be detected. (b) DDPs (in the inset) of the $\text{Ce}_{0.2}\text{Zr}_{0.8}\text{O}_2$ particle (2) and $\theta\text{-Al}_2\text{O}_3$ crystallite (1) show a perfect alignment of $(002)_{\text{CZ}}$ and $(002)_{\theta}$ planes, (arrowed).

comparison of these DDP quantitative features with those corresponding to both alumina and CZMO phases allowed distinguishing the precise nature of the particles detected in HREM images. As far as CZMOs are concerned, the monoclinic phase is easily differentiated from the cubic and tetragonal ones. On the other hand, the discrimination between tetragonal and cubic phases is more complicated or may become even impossible for very tiny (smaller than a few nm) crystallites.⁵⁰ Nevertheless, the presence of (001) reflections in the DDPs, with spacing around 0.52 nm, which is forbidden in the cubic phases, allows detecting the presence of tetragonal CZ20 particles, as shown in Figure 6b. Using this reliable discrimination criterion, a significant number of CZ20 particles exhibiting tetragonal features, and with diameters ranging from 9 to 20 nm, have been unequivocally identified, whereas no evidence of monoclinic CZ20 crystallites was obtained.

Regarding the structure of the support phase after the aging treatment, HREM images reveal the presence of well crystallized alumina particles the sizes of which range up to a few tens of nanometers. DDPs corresponding to these particles show reflections which unambiguously correspond to a $\theta\text{-Al}_2\text{O}_3$ phase (Figure 7a).

A perusal of the HREM data has revealed in a few cases the presence of orientation relationships between

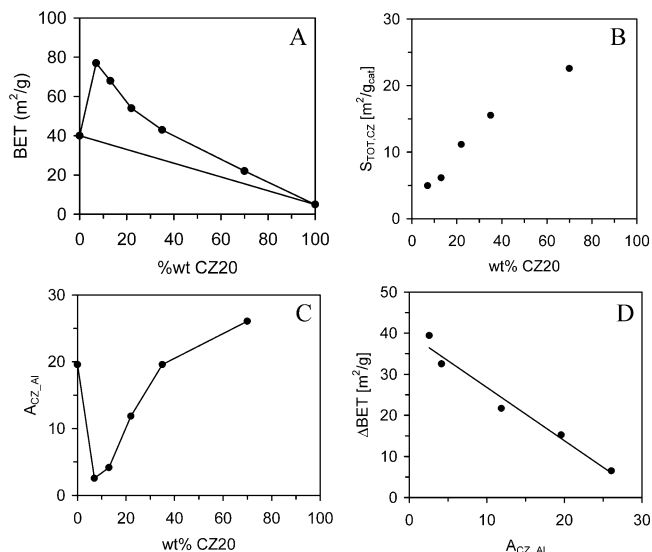


Figure 8. (A) BET area of $\text{Ce}_{0.2}\text{Zr}_{0.8}\text{O}_2(\text{YY}) / \text{Al}_2\text{O}_3$ samples calcined at 1373 K for 5 h (the straight line represents the BET area of a non-interacting physical mixture); (B) calculated total geometrical area of the $\text{Ce}_{0.2}\text{Zr}_{0.8}\text{O}_2$ phase (data calculated as reported in the appendix (Supporting Information) assuming a spherical model for the particles); (C) degree of $\text{Ce}_{0.2}\text{Zr}_{0.8}\text{O}_2(\text{YY}) / \text{Al}_2\text{O}_3$ aggregation as a function of $\text{Ce}_{0.2}\text{Zr}_{0.8}\text{O}_2$ loading; and (d) degree of BET area stabilization (ΔBET) vs degree of aggregation. The line is added as an eye-guide.

CZ20 particles and the support in contact with them. As depicted in the insets of Figure 7b, the DDPs of the CZ20 particle and that of the neighboring Al_2O_3 crystallite show a perfect alignment of (002) planes of tetragonal CZ20 and (002) planes of $\theta\text{-Al}_2\text{O}_3$.

3.5. Effect of $\text{Ce}_{0.2}\text{Zr}_{0.8}\text{O}_2$ Loading on Textural Properties: Calcination and Hydrothermal Treatments. Having established the optimal CZMO composition leading to the highest stabilization of the system, the effects of varying the loading of the CZ20 phase on Al_2O_3 were analyzed. Five samples with CZ20 loading ranging from 7 to 70 wt % were used. As above-noted, a monolayer coverage of the CZ20 phase over the present alumina corresponds to a loading of ca. 43 wt %.

Both textural stability and CZMO crystallite size appear significantly affected by the amount of CZ20 phase loaded onto Al_2O_3 (Figure 8a and Table 2). There is synergic effect on both Al_2O_3 and CZ20 phases in that the crystallite sizes of the CZMO are always lower compared to unsupported $\text{Ce}_{0.2}\text{Zr}_{0.8}\text{O}_2$, and they increase with CZ20 content. In contrast, the crystallite size of Al_2O_3 decreases with increasing CZ20 content (Table 2). The BET values lie above the straight lines representing BET area of a non-interacting CZMO and Al_2O_3 , i.e., physical mixture, for CZ20 loading between 7 and 70 wt %. The maximum of the thermal stabilization is achieved for the CZ20(7)/ Al_2O_3 sample.

By considering a spherical geometrical model for the CZ20 and Al_2O_3 particles (compare Supporting Information for calculations) and using the crystallite sizes detected from XRD, the total geometrical area of the CZ20 particles per gram of the catalyst can be calculated (Figure 8b). Notice that such a calculation assumes a non-aggregated state of the CZ20 particles, i.e., the dimensions of the crystalline domain (crystallite size) as detected by XRD and the CZ20 particle size are equal.

(50) Baker, R. T.; Bernal, S.; Lopez-Cartes, C.; Perez-Omil, J. A.; Montardi, Y. *Inst. Phys. Conf. Ser.* **1999**, *161*, 521.

Table 2. Results of Structural Characterization of $Ce_{0.2}Zr_{0.8}O_2$ (YYwt %)/ Al_2O_3 Samples

$Ce_{0.2}Zr_{0.8}O_2$ content/wt %	phase distribution/wt %			Al_2O_3 particle size (nm)	structural parameters of the $Ce_{0.2}Zr_{0.8}O_2$ phase							
	$Ce_{0.2}Zr_{0.8}O_2$	$\theta-Al_2O_3$	$\alpha-Al_2O_3$		a (Å)	c (Å)	V (Å ³)	c/a^a	particle size (nm)	R_{wp}^b	R_p^b	R_f^b
0		65	35	13								
7	5	95		13	3.627(2)	5.229(3)	68.79	1.019	10	10.9	8.4	1.4
13	13	87		12	3.6277(6)	5.2285(9)	68.81	1.019	15	8.6	6.5	0.8
22	21	79		10	3.6333(3)	5.2374(7)	69.14	1.019	14	9.9	7.4	0.8
35	36	64		9	3.6387(2)	5.2403(4)	69.38	1.018	16	8.6	6.4	1.2
70	67	33		8	3.6410(1)	5.2432(2)	69.51	1.018	22	10.6	8.5	0.8
100	100				3.6446(2)	5.2458(2)	69.68	1.018	23	10.8	7.4	1.3

^a $a' = a \times \sqrt{2}$. ^b Where

$$R_p = \frac{\sum |y_i(\text{obs}) - y_i(\text{calc})|}{\sum y_i(\text{obs})} \quad (R\text{-pattern}), \quad R_{wp} = \left\{ \frac{\sum w_i(y_i(\text{obs}) - y_i(\text{calc}))^2}{\sum w_i(y_i(\text{obs}))^2} \right\}^{1/2} \quad (R\text{-weighted pattern}), \quad \text{and } R_f = \frac{\sum |(I_K(\text{obs}))^{1/2} - (I_K(\text{calc}))^{1/2}|}{\sum (I_K(\text{obs}))^{1/2}} \quad (R\text{-structure factor}).$$

This is a reasonable assumption: comparable dimensions of the CZ20 particles were detected by both XRD and HREM; further, the probability that CZ20 crystallites may reciprocally interact to a significant degree is quite low. A ratio of CZ20 to Al_2O_3 particles of $2.1 \pm 0.5:100$ is calculated from the XRD data for all the CZ20-(YY)/ Al_2O_3 samples, which is in agreement with the above suggestion.

The total geometrical area of the CZ20 phase monotonically increases with the CZ20 loading, which is the exact opposite with respect to the observed BET stabilization. This indicates that the aggregation of the crystallites, rather than a simple interfacial contact, plays a key role in the BET area stabilization. This is confirmed by the data reported in Figure 8c and d, which show that: (1) the lowest degree of aggregation is achieved in the CZ20(7)/ Al_2O_3 sample; and (2) the degree of mutual stabilization (Δ BET), calculated as increase of BET area with respect to that of a physical mixture, is linearly related to the degree of aggregation of the system. Worth noting is the degree by which the aggregation of the system is affected by the loading of the CZ20 phase: for a 5-fold decrease of CZ20 loading (from 35 to 7 wt %), the degree of agglomeration decreased by a factor of 10, resulting in an increase of surface area of about $35 \text{ m}^2 \text{ g}^{-1}$. For sake of comparison, Piras et al.³⁷ found almost no variation of the BET surface area in $CeO_2-Al_2O_3$ composite materials calcined at 1373 K as the CeO_2 content was varied from 3 to 15 wt %. Similarly, constant surface areas were observed for ZrO_2 loading between 0.43 and 14.8 wt % on impregnated $ZrO_2-Al_2O_3$ systems after calcination at 1373 K.³² This clearly points out a synergic stabilization of the textural properties due to the simultaneous presence both the Zr and Ce component in the present nanocomposite systems.

Summarizing this part, the analysis of the textural properties suggests a clear effect of the added CZ20 phase on the degree of aggregation of this nanocomposite phase, with the lowest CZ20 loading among those investigated (7 wt %) being the most efficient in preventing the aggregation.

As suggested by a referee, selected aging experiments were performed under hydrothermal conditions, which are known to favor the rate of sintering,⁵¹ in order to

assess the general validity of the present findings under conditions that reflect more closely those of the real TWC applications. Remarkably, no appreciable effect of water addition was detected on either CZ20(7)/ Al_2O_3 or CZ20(35)/ Al_2O_3 for treatments performed at 1273 K for 5 h with respect to calcination: surface areas of 120 and $105 \text{ m}^2 \text{ g}^{-1}$, and 112 and $87 \text{ m}^2 \text{ g}^{-1}$ were measured over the two samples, respectively, after the hydrothermal and calcination treatments. For comparison, Yao et al. found a BET area of $56 \text{ m}^2 \text{ g}^{-1}$ for a 30 wt % $Ce_{0.2}Zr_{0.8}O_2/Al_2O_3$ system prepared by an incipient wetness of nitrate precursors after aging under hydrothermal conditions at 1273 K for 4 h.¹⁹ The important aspect is that not only is the BET area preserved in the presence of H_2O in comparison to the calcination, but also the migration of the CZMO species over the Al_2O_3 is not influenced by the presence of H_2O : particle sizes of 6 and 7 nm were detected by XRD respectively in the presence and absence of H_2O after the treatment at 1273 K over CZ20(7)/ Al_2O_3 , whereas values of 8 and 10 nm were observed over sample CZ20(35)/ Al_2O_3 .

Increasing the temperature of the hydrothermal treatment up to 1393 K, remarkably high BET areas of 67 and $50 \text{ m}^2 \text{ g}^{-1}$ were measured over CZ20(7)/ Al_2O_3 and CZ20(35)/ Al_2O_3 , respectively, indicating no effects of water addition on thermal stability under our conditions. This unequivocally confirms the remarkably high thermal stability of the present samples.

3.6. Effect of $Ce_{0.2}Zr_{0.8}O_2$ Loading on Structural Properties of CZ20(YY)/ Al_2O_3 . The CZ20(YY)/ Al_2O_3 and CZ20 sample were analyzed by performing a Rietveld fitting of the XRD patterns of samples calcined at 1373 K for 5 h. The presence of Ce(III) was detected by means of XANES spectroscopy.

Space groups $R\bar{3}c$, $C2/m$, and $P4_2/nmc$ were used for the $\alpha-Al_2O_3$, $\theta-Al_2O_3$, and CZ20, respectively, for the Rietveld refinement. The results are reported in Table 2. Reliable R_{wp} , R_p , and R_f factors⁵² were obtained for all the samples. The XRD spectra were fitted with a single phase CZ20 solid solution with a tetragonality of $c/a' = 1.018-1.019$, where $a' = a \times \sqrt{2}$ in all the

(51) Pijolat, M.; Dauzat, M.; Soustelle, M. *Solid State Ionics* **1992**, *50*, 31.

(52) Izumi, F. J. *Ceram. Soc. Jpn.* **2001**, *111*, 617.

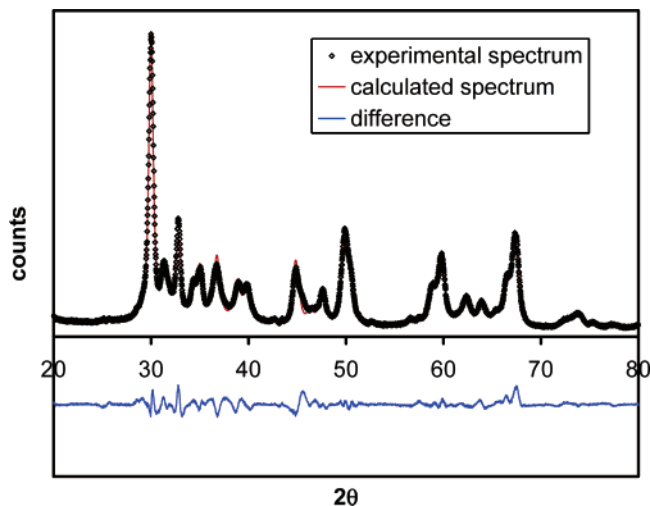


Figure 9. Profile fitting of the experimental XRD pattern of $\text{Ce}_{0.2}\text{Zr}_{0.8}\text{O}_2(13 \text{ wt } \%) / \text{Al}_2\text{O}_3$ calcined at 1373 K for 5 h using the Rietveld method.

CZ20(YY)/ Al_2O_3 samples. Such structural parameters are consistent for this CZMO composition.⁵³ The Zr^{4+} (Ce^{4+}) and O^{2-} ions were located at respectively the $2a$ and $4d$ special positions of the $P4_2/nmc$ space group. In the calculation, we assumed that the cation sites are randomly occupied by 80% Zr and 20% Ce atoms. An example of such fitting is reported in Figure 9.

A perusal of the structural parameters reported in Table 2 reveals that a noticeable effect on the structural properties of the CZ20 phase is induced by the interaction with Al_2O_3 , which depends on the amount of the CZ20 phase loaded over the Al_2O_3 phase. There is a significant contraction of the cell volume due to the decrease of cell parameter and an increase of both anion and cation atom disorder as the amount of CZ20 loaded is decreased, particularly in the range 35 to 7 wt %, as illustrated in Figure 10. No appreciable change of tetragonality is detected.

Generally speaking, when the ions constituting a solid solution feature different ionic radii, the Vegard rule may be applied, which shows that the cell parameter is a linear function of the composition. For CeO_2 and ZrO_2 based systems a number of semi-empirical or empirical models have been reported to quantitatively evaluate this variation of the cell parameter.^{54–57} Ce(IV) , Zr(IV) , and Al(III) feature ionic radii of 0.097, 0.084, and 0.053 nm, respectively.⁵⁸ To account for the observed decrease of the cell parameters, one can consider that either Ce(IV) is lost from the CZ20 lattice (model I) or Al(III) is dissolved in the solid solution substituting Ce(IV) (model II), or both. Further to consider is the fact that CeO_2 highly dispersed on Al_2O_3 is known to strongly interact with Al_2O_3 , forming surface Ce(III) species, and/or CeAlO_3 .¹³ It can be therefore expected that if part of ceria is not incorporated into the solid solution with

ZrO_2 , this can interact with the surface of Al_2O_3 , presumably leading to Ce(III) species. XANES measurements were therefore performed at the L_{III} edge on the samples calcined at 1273 K to quantitatively detect the amount of Ce(III) species in the system.^{7,59} The results reported in Figure 11 show that a significant fraction, with respect to the solid solution, of the ceria species is detected as Ce(III) species, suggesting their interaction with the Al_2O_3 phase rather than being incorporated into $\text{Ce}_{0.2}\text{Zr}_{0.8}\text{O}_2$. Consistently, no evidence for Ce(III) species was detected in a reference $\text{Ce}_{0.2}\text{Zr}_{0.8}\text{O}_2$. Noticeably, the relative extent of ceria species, presumably interacting with Al_2O_3 , increases with decreasing the loading of the supported phase, in line with the decrease of the cell parameters.

To evaluate the consistency of the hypothesis that shrinking of the cell parameter is due to loss of ceria out of the solid solution lattice (model I), we have calculated the cell parameters for the solid solution applying an ion packing model derived by Yashima et al.^{55,56} for fluorite type of solids [The general validity of the ion packing model for predicting the cell parameter of doped ternary–quaternary CeO_2 – ZrO_2 solid solutions has been verified for over 30 different compositions (Di Monte et al. paper in preparation)]. Briefly, the cell parameter is calculated in this model by considering the average cation and anion radii using the Shannon's radii,⁵⁸ which then are substituted in eq 2 to calculate the cell parameter of the cubic face centered cell, i.e., a fluorite type of oxide.

$$a = \frac{4}{\sqrt{3}}(r_{\text{cation}} + r_{\text{anion}}) \quad (2)$$

The relationship between the pseudocubic (derived from tetragonal $P4_2/nmc$) and cubic ($Fm3m$) cells may be easily derived through the use of cell volume of the fluorite unit cell

$$\text{Cell Volume} = (a \times \sqrt{2})^2 \times c$$

where a and c are the tetragonal cell parameters.

The amount of cerium species “missing” in the solid solution evaluated on the basis of such calculations is compared with the amount of Ce(III) species detected by XANES measurements in Figure 11. [A full discussion of the XANES results and the methodology employed to evaluate the Ce(III) content will be reported in a forthcoming paper. The reliability of the Ce(III) evaluation was cross-checked using magnetic susceptibility measurements.] The calculated content for Ce(III) species is significantly higher than the experimental Ce(III) values, which suggests that a more complex interaction occurs.

Zirconia and alumina show a tendency to mix together.^{60,61} On the other hand, replacement of cerium with aluminum species may both release the stress, which is generated in the ZrO_2 lattice by insertion of the large cerium cation, and form, by interaction with

(53) Yashima, M.; Hirose, T.; Katano, S.; Suzuki, Y.; Kakihana, M.; Yoshimura, M. *Phys. Rev. B: Condens. Matter Mater. Phys.* **1995**, *51*, 8018.

(54) Hong, S. J.; Virkar, A. V. *J. Am. Ceram. Soc.* **1995**, *78*, 433.

(55) Yashima, M.; Ishizawa, N.; Yoshimura, M. *J. Am. Ceram. Soc.* **1992**, *75*, 1550.

(56) Yashima, M.; Ishizawa, N.; Yoshimura, M. *J. Am. Ceram. Soc.* **1992**, *75*, 1541.

(57) Kim, D. J. *J. Am. Ceram. Soc.* **1989**, *72*, 1415.

(58) Shannon, R. D. *Acta Crystallogr.* **1976**, *A32*, 751.

(59) Overbury, S. H.; Huntley, D. R.; Mullins, D. R.; Glavee, G. N. *Catal. Lett.* **1998**, *51*, 133.

(60) Faro, A. C.; Souza, K. R.; Camorim, V. L. D. L.; Cardoso, M. B. *Phys. Chem. Chem. Phys.* **2003**, *5*, 1932.

(61) Faro, A. C.; Souza, K. R.; Eon, J. G.; Leitao, A. A.; Rocha, A. B.; Capaz, R. B. *Phys. Chem. Chem. Phys.* **2003**, *5*, 3811.

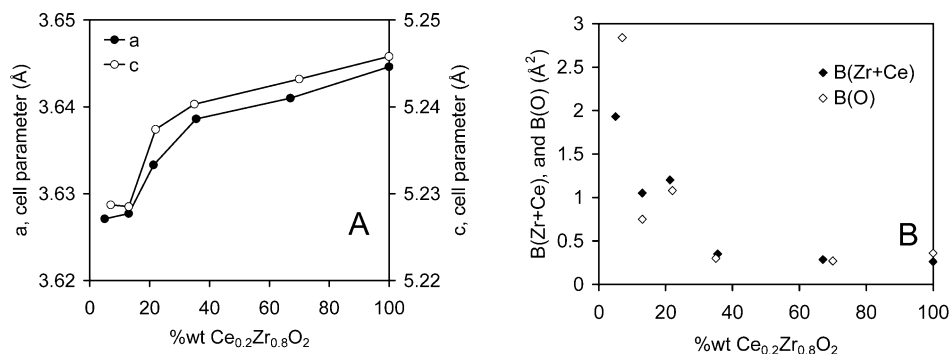


Figure 10. Variation of cell parameter (A) and structural B factor (B) as a function of $Ce_{0.2}Zr_{0.8}O_2$ content in $Ce_{0.2}Zr_{0.8}O_2$ (YY wt %)/ Al_2O_3 .

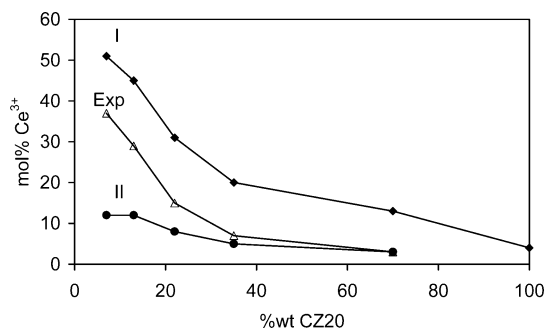
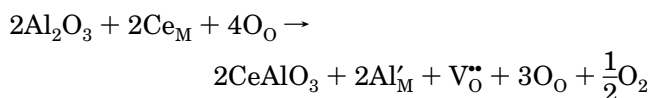


Figure 11. Calculated, using an ion packing model (model I and II – see text), and experimental $Ce(III)$ content in the $Ce_{0.2}Zr_{0.8}O_2$ (YY wt %)/ Al_2O_3 samples as a function of $Ce_{0.2}Zr_{0.8}O_2$ (CZ20) loading.

Al_2O_3 , a cerium aluminate, leading to the stabilization of the system (model II). Consistently, mutual mixing of cerium and alumina species has also been detected.⁶² Such a complex interaction can be described using the Kröger–Vink notation by supposing that a fraction of Al_2O_3 reacts with the solid solution according to the following reaction:



where $M = Ce$ or Zr , and Ce_M , O_O , Al'_M , and $V_O^{\bullet\bullet}$ represent, respectively, a cerium cation in an M lattice site, an oxygen atom in an anion lattice site, an aluminum ion substituting one M lattice site (negatively charged with respect to the lattice), and a doubly charged (positive with respect to the lattice) oxygen vacancy.

Noticeably, when such a reaction network is considered, even a very small degree of substitution, i.e., $Ce(III)$, can easily account for the observed decrease of cell parameter (Figure 11). On the basis of the present evidence, we obviously cannot attribute the cell contraction to a single mechanism, but it is worth noting that the above considerations suggest excluding a simple ceria–alumina interaction as the only interaction between the $CZ20$ and Al_2O_3 phases in the present system. A more complex network of mutual interactions needs to be considered to take into account the observed phenomena.

3.7. A Rationale for the $Ce_xZr_{1-x}O_2/Al_2O_3$ Stabilization. An attempt to develop a rationale for the thermal stabilization of the nanocomposite $CZXX/Al_2O_3$ system should consider a number of factors that have been addressed in the present paper. First of all, the added $CZMO$ phase slows down the kinetics of transitional Al_2O_3 phase transformation in the present systems. However, this effect appears to be limited to the $\theta \rightarrow \alpha$ transformation, with the $\gamma \rightarrow \delta/\theta$ transformation being nearly unaffected, except for the ZrO_2 and $CZ20$ containing systems.

To rationalize this aspect, it is convenient to recall the structural aspects of these phase transitions. $\gamma-Al_2O_3$ assumes a spinel type structure (space group $Fd\bar{3}m$), where the oxygen anions pack in the (111) plane to create an ABCABC sequence, whereas the packing of the aluminum cations can be described by two alternating layers: (1) a layer containing only octahedrally coordinated cations and (2) layers containing aluminum both in octahedral and tetrahedral coordination.^{63,64} Generally speaking, there is discrete cation disorder in the γ phase, also due to the presence of cation vacancies related to the presence of hydroxyls at the surface of the solid. The disordered nature of this phase therefore suggests that formation of interfaces structurally coherent with the $CZMO$ phase⁶⁵ is not favored; accordingly, the disappearance of $\gamma-Al_2O_3$ which occurs via nucleation of the $\delta-Al_2O_3$ is almost unaffected by the $CZMO$ component.

Even though the other transitional aluminas formed from $\gamma-Al_2O_3$ upon thermal treatment feature different space group symmetry— $\delta-Al_2O_3$ has been described as a superlattice (triple spinel unit cell, $P4m2$ space group) with cation vacancies distributed over the octahedral sites, whereas $\theta-Al_2O_3$ adopts a monoclinic symmetry and is structurally isomorphous with $\beta-Ga_2O_3$ (space group $C2/m$)—all these structures can be related to the fcc packing of oxygen anions, where phase transformations occur via a progressive ordering of the aluminum cations in the interstitial sites of this packing, leading to a system where they are equally distributed over the octahedral and tetrahedral sites ($\theta-Al_2O_3$).⁶³ Consistently, the most dense (111) γ plane is preserved in the $\gamma-Al_2O_3$ transformation, with the corresponding spacing in $\theta-Al_2O_3$ being the (201) θ , which presents a small

(63) Levin, I.; Brandon, D. *J. Am. Ceram. Soc.* **1998**, *81*, 1995.

(64) Zhou, R. S.; Snyder, R. L. *Acta Crystallogr., Sect. B: Struct. Sci.* **1991**, *47*, 617.

(65) Oudet, F.; Courtine, P.; Vejun, A. *J. Catal.* **1988**, *114*, 112.

(62) Sasikala, R.; Sudarsan, V.; Kulshreshtha, S. K. *J. Solid State Chem.* **2002**, *169*, 113.

shrinkage of the plane distance from 0.4579 to 0.4539 nm.

At variance, the structure of α - Al_2O_3 is based on the *hcp* packing of oxygen anions, indicating the oxygen rearrangements must occur to form this phase. Nucleation, followed by growth of individual crystals of α - Al_2O_3 is suggested as a mechanism for this transformation.

This is an important point, since it suggests that thermal stabilization could be achieved if oxygen rearrangement can be blocked by, for example, some structural coherence of the supported phase. This factor has in fact often been invoked for textural stabilization of doped aluminas.⁶⁵ In this respect, it is worth noting that considering a pseudocubic superlattice for the CZMO phases consisting of 3a, 3b, and 3c pseudocubic lattice parameters, we calculate a $d(222)$ spacing of 0.4441, 0.4489, 0.4601, 0.4648, and 0.4689 nm for, respectively, CZ0, CZ20, CZ60, CZ80, and CZ100 phases. Both CZ20 and CZ60 therefore would present the minor deviations for coherent orientation of such planes with those above quoted for alumina. As shown in section 3.5, some evidence has in fact been found for some structural coherence between the plane orientation on the CZ20 and θ - Al_2O_3 phase. We also notice that the interplane spacing is 0.273 nm for (002) in $\text{Ce}_{0.2}\text{Zr}_{0.8}\text{O}_2$ and 0.262 nm for (002) θ - Al_2O_3 , which corresponds to a relatively small (4.0%) misfit. We have to admit that a full dedicated HREM work, which would provide statistically relevant data, was not within the scope of the present paper, accordingly, we cannot unequivocally discard or support the structural coherence as the driving force for thermal stabilization of Al_2O_3 .

In fact, the intergrowth of the CZ20 and Al_2O_3 particles, which would be responsible for thermal stabilization of Al_2O_3 , should be favored at increasing calcination temperatures where crystallization of the CZ20 phase and simultaneous ordering of the alumina phase occur, favoring mutual interaction in the composite material. Phase segregation observed for the CZ60 phase would disrupt this structural coherence, leading to a poorer stabilization of the system, as in fact found. On the other hand, the (002) interplane spacing is 0.271 nm in CeO_2 , which corresponds to a negligible misfit when compared to θ - Al_2O_3 interplane spacing; however, the CZ100(13)/ Al_2O_3 is far less thermally stable compared to CZ20(13)/ Al_2O_3 as indicated by detection of α - Al_2O_3 after calcination at 1373 K.

We have attempted to further check this point by preparing a CZ20(13)/ Al_2O_3 sample using an Al_2O_3 that has been calcined at 1173 K for 20 h, before supporting the CZ20 phase. As checked by XRD, such an initial calcination leads to a mixture of approximately 50% of γ , the remaining being δ/θ phase. Obviously, the longer calcination time and higher temperature lead to a lower initial BET surface area for the latter samples (165 vs 186 $\text{m}^2 \text{g}^{-1}$). Textural stability was therefore compared in terms of relative stability of the BET area with calcination (Figure 12). Except for the calcination at 1273 K, no appreciable difference in the sintering behavior was detected between the two samples, suggesting a minor role of a structural coherence in thermal stabilization of the present systems. This interpretation

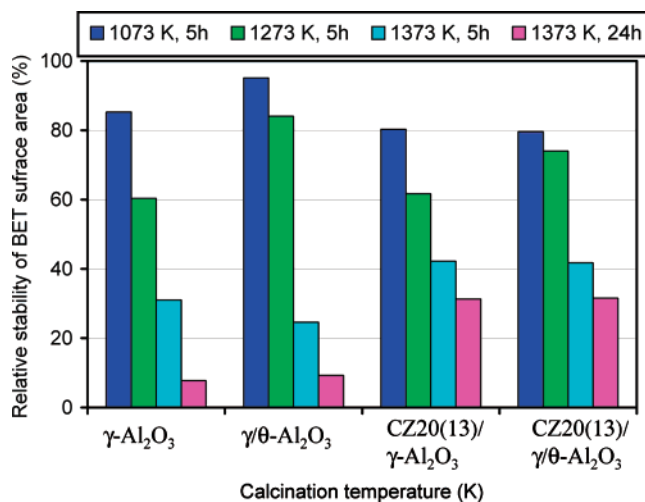


Figure 12. Effects of calcination temperature on the relative BET surface area stability (calculated as $\text{BET}_{\text{XX}}/\text{BET}_{\text{Fresh}} \times 100$, where XX represents the calcination temperature) in $\text{Ce}_{0.2}\text{Zr}_{0.8}\text{O}_2$ (13 wt %)/ γ - Al_2O_3 and $\text{Ce}_{0.2}\text{Zr}_{0.8}\text{O}_2$ (13 wt %)/ δ/θ - Al_2O_3 samples (compare text for details).

appears well in line with a very recent report showing that thermal stabilization of Al_2O_3 with La is prevalently related to selective doping on single atom surface sites of the Al_2O_3 , segregation in bulk of the dopant, or their clustering being unfavored.⁶⁶ On the other hand, this situation may hold for three-valent dopants such as Ce(III) or La(III), whereas for systems with different valency, such as Zr(IV) in our case, the situation may be different.³²

However, this appears to be only one of the multifaceted aspects of the CZMO- Al_2O_3 interaction. Both the Rietveld and XANES data (section 3.6) indicate that mutual solubility of the cations must also play a significant role in thermal stabilization. Whereas evidence for patches of CeAlO_3 were not detected in the present samples (also due to relatively small absolute amount of Ce(III) species), we must notice that dissolution of some Zr species into γ - Al_2O_3 has recently been detected by XAS in a $\text{ZrO}_2/\text{Al}_2\text{O}_3$ composite material prepared by an impregnation technique.⁶⁰ This could also account for the stabilization of the γ - Al_2O_3 observed in the Zr-rich domains of the CZMO phases. The reciprocal solubilization of the Zr and Al species in the lattice that is detected upon such high-temperature calcination is somewhat surprising as it is well-known that due to the reciprocal insolubility of these cations, ZrO_2 - Al_2O_3 solid solutions are metastable materials which expel alumina to grain boundaries on high temperature heating.^{67,68}

A very important result of the present paper is, however, the observation that sintering of the $\text{Ce}_x\text{Zr}_{1-x}\text{O}_2$ particles is strongly retarded by the interaction of the $\text{Ce}_x\text{Zr}_{1-x}\text{O}_2$ phase with Al_2O_3 . $\text{Ce}_{0.2}\text{Zr}_{0.8}\text{O}_2$ featured particle sizes of 8 and 35 nm after calcination at 973 and 1373 K, respectively, for 5 h, corresponding to a 4.4-

(66) Wang, S. W.; Borisevich, A. Y.; Rashkeev, S. N.; Glazoff, M. V.; Sohlberg, K.; Pennycook, S. J.; Pantelides, S. T. *Nat. Mater.* **2004**, *3*, 143.

(67) Stough, M. A.; Hellmann, J. R. *J. Am. Ceram. Soc.* **2002**, *85*, 2895.

(68) Gao, L.; Liu, Q.; Hong, J. S.; Miyamoto, H.; De la Torre, S. D.; Kakitsuji, A.; Liddell, K.; Thompson, D. P. *J. Mater. Sci.* **1998**, *33*, 1399.

fold increase. In comparison, 2.2- and 3.3-fold increases of $Ce_{0.2}Zr_{0.8}O_2$ and CeO_2 particle size are observed in the CZ20(13)/ Al_2O_3 and CZ100/ Al_2O_3 , respectively, for equal calcination. This highlights the critical role of both doping the CeO_2 phase with ZrO_2 and supporting it on Al_2O_3 in order to confer thermal stability to the $Ce_xZr_{1-x}O_2$ phase. The structural coherence as detected by HREM may not be directly responsible for these effects, however, it should be noticed that intermixing of $Ce_{0.2}Zr_{0.8}O_2$ and Al_2O_3 phases as indicated by the present results is certainly favored by coherent growth of the particles and this may be a prerequisite for such phenomena. The present results appear nicely in line with a recent computational study showing that supporting a thin film of CeO_2 on an oriented Y_2O_3/ZrO_2 surface strongly modifies the structure of the supported CeO_2 : the exposure of more reactive surfaces ((100) or (110) vs (111)), cation mixing at the interface, and generation of defective sites due to coherent CeO_2 grain growth are all favored.⁶⁹ As it will be shown in a forthcoming paper,⁷⁰ stabilization of the present nanodispersed $Ce_xZr_{1-x}O_2$ phase at the Al_2O_3 surface leads to a fairly high improvement of the redox properties of these materials with respect to Al_2O_3 free systems, the extent of which is related to the degree of mutual interaction, as detected in the present work.

4. Conclusions

The investigation of thermal stability of $Ce_xZr_{1-x}O_2/Al_2O_3$ systems prepared by impregnation showed that important interactions between the $Ce_xZr_{1-x}O_2$ and Al_2O_3 systems are induced by calcination at high temperatures, leading to remarkably high thermal stabilities, despite the use of a very simple and inexpensive synthesis methodology. HREM, Rietveld, and XANES analysis of the present $Ce_{0.2}Zr_{0.8}O_2/Al_2O_3$ system revealed a very complex nature of these mutual interactions where observation of orientation relationships and reciprocal ion dissolution occur after high-temperature calcination. Evidence was obtained that the ratio of ZrO_2/CeO_2 in the mix plays a role in the interaction with the Al_2O_3 phase: high ZrO_2 contents stabilize γ - Al_2O_3 , whereas high CeO_2 contents stabilize exclusively the θ - and δ - Al_2O_3 phases. Despite the relatively low and constant ratio of $Ce_{0.2}Zr_{0.8}O_2/Al_2O_3$ particles, the degree of agglomeration appears dramatically affected by the amount of the $Ce_{0.2}Zr_{0.8}O_2$ phase. Both the Zr and Ce component appear to act synergically as thermal sta-

bilizing agents of the nanocomposite CeO_2 - ZrO_2 - Al_2O_3 material. The observation that the highest degree of thermal stabilization is achieved at the lowest $Ce_{0.2}Zr_{0.8}O_2$ loading suggests that some highly dispersed dopant species can contribute to this thermal stabilization of Al_2O_3 .⁶⁶

A critical role of the following factors concerning the preparation of these nanocomposite oxide has been identified: (1) loading and composition of the $Ce_xZr_{1-x}O_2$ phase, with high ZrO_2 contents favoring higher thermal stability compared to CeO_2 -rich systems; and (2) use of appropriate $Ce_xZr_{1-x}O_2$ precursors: citrate precursors with respect to commonly employed nitrates.

In summary, the achieved thermal stabilities appear to be comparable to or even better than those achieved by complex synthesis methodologies;¹⁵ single-phase nanosized $Ce_xZr_{1-x}O_2$ solid solutions in close contact with an Al_2O_3 matrix could be obtained here for calcination temperatures as high as 1373 K, without concomitant α - Al_2O_3 formation. To our knowledge, only cogelling of Ce, Zr, and Al isopropoxides/acetylacetonates produced materials where a higher degree of interaction between the various phases could be achieved, as denoted by stabilization of γ - Al_2O_3 for temperatures as high as 1373 K,¹⁸ yet the complex and expensive procedure makes such methodology unacceptable with respect to cost for a wide range of industrial production as these materials nowadays experience. Finally, excellent hydrothermal stability was found for some of the materials investigated, suggesting a more general applicability of the present findings.

Acknowledgment. Professor Serafin Bernal, University of Cadiz, is gratefully acknowledged for his support and helpful discussions. Professor Francesco Princivalle, University of Trieste, is gratefully acknowledged for his continuous support and valuable help with the XRD measurements. Prof. Mauro Graziani, University of Trieste, is acknowledged for helpful discussion. R.D.M. thanks University of Trieste for supporting her position. MURST-PRIN 2002- project "Stabilisation under reaction conditions of catalysts based on nanodispersed metals for use in selective oxidation reactions", Regione F.V.G., Azione Integrata Italy-Spain HI-2000-0193 and IT355, MEL Chemicals and University of Trieste-Fondo ex 60% are acknowledged for financial support.

Supporting Information Available: Calculation of the data reported in Figure 8 (pdf file). This material is available free of charge via the Internet at <http://pubs.acs.org>.

CM048829Q

(69) Sayle, D. C.; Maicaneanu, S. A.; Watson, G. W. *J. Am. Chem. Soc.* **2002**, *124*, 11429.

(70) Di Monte, R.; Montini, T.; Fornasiero, P.; Kašpar, J.; Fonda, E. paper to be submitted.